

SSL4EO-S12: A Large-Scale Multi-Modal, Multi-Temporal Dataset for Self-Supervised Learning in Earth Observation

Yi Wang, *Student Member, IEEE*, Nassim Ait Ali Braham, Zhitong Xiong, *Member, IEEE*, Chenying Liu, Conrad M Albrecht, *Member, IEEE*, Xiao Xiang Zhu, *Fellow, IEEE*

Abstract—Self-supervised pre-training bears potential to generate expressive representations without human annotation. Most pre-training in Earth observation (EO) are based on ImageNet or medium-size, labeled remote sensing (RS) datasets. We share an unlabeled RS dataset SSL4EO-S12:

Self-Supervised Learning for Earth Observation - Sentinel-1/2 to assemble a large-scale, global, multimodal, and multi-seasonal corpus of satellite imagery from the ESA Sentinel-1 & -2 satellite missions. For EO applications we demonstrate SSL4EO-S12 to succeed in self-supervised pre-training for a set of methods: MoCo-v2, DINO, MAE, and data2vec. Resulting models yield downstream performance close to, or surpassing accuracy measures of supervised learning. In addition, pre-training on SSL4EO-S12 excels compared to existing datasets. We make openly available the dataset, related source code, and pre-trained models at <https://github.com/zhu-xlab/SSL4EO-S12>.

Index Terms—Self-supervised learning, remote sensing, dataset, benchmark, Sentinel-1/2.

I. INTRODUCTION

IN recent years, self-supervised learning did contribute to significant breakthroughs in computer vision [1]. Self-supervised learning methods are tailored to exploit massive amounts of unlabeled data to pre-train general purpose models such to greatly improve generalizability and label efficiency on downstream applications compared to training from scratch.

The success of self-supervised representation learning did attract attention within the remote sensing community where large-scale, annotated datasets [2] are difficult to assemble with petabytes of unlabeled Earth observation (EO) data available. In fact, numerous studies in the remote sensing (RS) literature prove the potential of self-supervised learning for a variety of problems, such as: scene classification [3, 4, 5], semantic segmentation [6], change detection [7], etc. Moreover, applications of SSL went far beyond processing of colored, three-channel RGB images, demonstrating promising results on multi-spectral [8], Synthetic Aperture Radar (SAR) [9], and hyperspectral data [10].

Despite the focus self-supervised learning for EO receives, only limited effort is dedicated to provide a large-scale dataset for pre-training. On the one hand, relying on computer vision datasets like ImageNet [11] is not a preferred option due to the domain gap between natural vs. satellite imagery modalities. On the other hand, most annotated EO datasets

like BigEarthNet [12] are limited in scale, restricted in spatial coverage, and do obey a task-specific class distribution. In addition, while there exist global datasets like SEN12MS [13] or SeCo [4], those are limited by patch overlap, sparse geographical distribution, or lack diversity in seasonal or multimodal information. Therefore, we invest effort towards the availability of EO-specific, pre-training datasets.

In this work, we introduce a new large-scale, globally distributed, multi-temporal and multi-sensor dataset *SSL4EO-S12: Self-Supervised Learning for Earth Observation - Sentinel-1/2*. The dataset consists of 3 million Sentinel-2 (multi-spectral, level-1C and level-2A) and Sentinel-1 (SAR) images of 250K locations sampled from all around the globe. Each location is provided with four snapshots from different seasons, allowing to capture variability within a calendar year. Additionally, we guarantee optimal geospatial coverage by avoiding overlap of the randomly sampled locations. This renders SSL4EO-S12 the largest and most global multi-spectral/SAR dataset in the remote sensing literature.

We demonstrate the potential of our dataset through a series of extensive experiments. Specifically, we evaluate four representative self-supervised learning algorithms—namely: MoCo [14], DINO [15], MAE [16], and data2vec [17]—on three different downstream tasks: scene classification, semantic segmentation and change detection. Our results indicate that pre-training on SSL4EO-S12 improves the performance compared to other existing datasets.

II. RELATED WORK

A. Self-supervised learning

Over past years, self-supervised learning did reach important milestones in computer vision narrowing the gap of unsupervised and supervised representation learning, especially through joint-embedding architectures. These methods get trained to promote similarity between augmented views of the same input, thereby enforcing invariance to data augmentation. Several families of such methods did emerge:

- *Contrastive methods* such as MoCo [14] and SimCLR [18] use negative pairs for which the representations are encouraged to be dissimilar;
- *Distillation methods* like BYOL [19] rely on an asymmetric teacher-student architecture;
- *Redundancy reduction methods* such as Barlow-Twins [20] decorrelate the dimensions of the embeddings at a batch level;

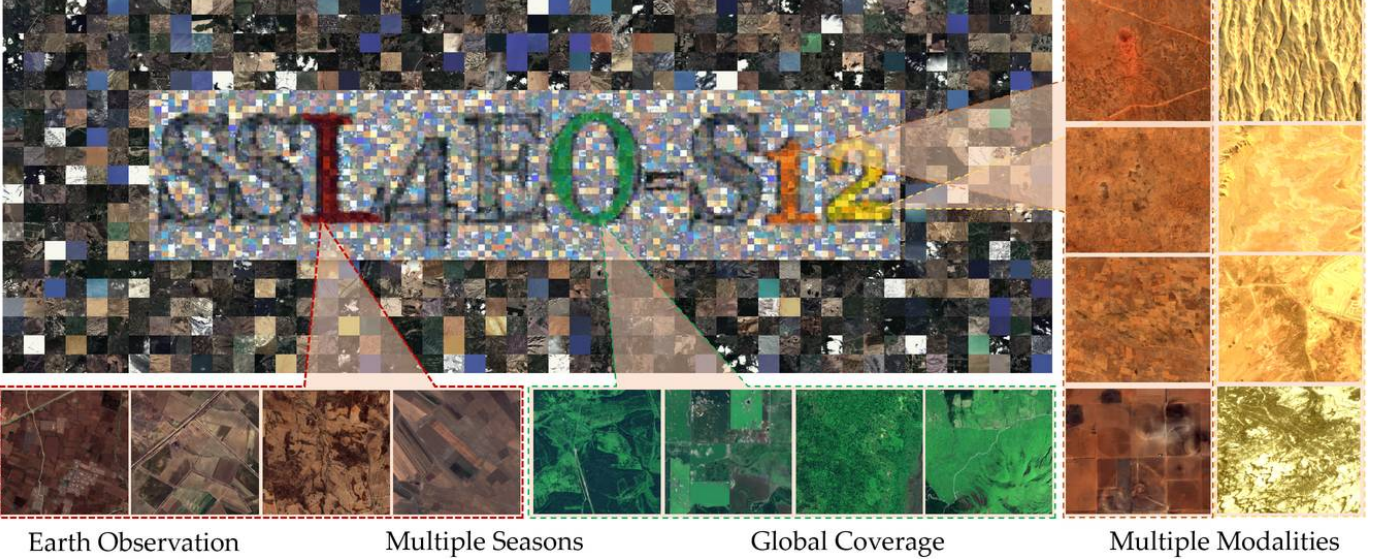


Fig. 1. Sample images of the SSL4EO-S12 dataset assembled.

- *Clustering-based methods* like SwAV [21] impose equipartition constraints.

In addition, recent developments in masked image modeling (MIM) reveal promising results. These methods reconstruct the masked parts of an input either at pixel-level [16], feature-level [17], or exploit visual tokens [22].

In this work, we benchmark four representative methods MoCo, DINO, MAE, and data2vec on the proposed dataset. This way, we cover a reasonably diverse set of representative methods from each model category: MoCo utilizes contrastive representative, DINO represents a distillation method, MAE is based on masked reconstruction, and data2Vec combines the masking mechanism with a joint-embedding architecture.

B. Datasets for pre-training

Pre-trained models on ImageNet are widely used for various computer vision tasks frequently providing benefits compared to training from scratch [23]. However, pre-training on ImageNet is less appropriate in the context of remote sensing:

- Single satellite image typically contains *many objects covering a large (geo)spatial area*—as opposed to object-centric datasets like ImageNet.
- Instead of 3-channel RGB imagery, there exist a plurality of sensors with *diverse spatial and spectral characteristics* in Earth observation.
- Due to *seasonal and time-of-the-day effects*, the temporal aspect of remote sensing measurements is key. E.g. geospatial locations yield variations in surface reflectance of electro-magnetic radiation depending on the time of acquisition.
- Labeled remote sensing datasets like BigEarthNet [12] bear *limitations* for self-supervised pre-training wrt. *scale of data, class distribution, and geospatial coverage*.

Consequently, there is need for large-scale pre-training datasets in remote sensing analytics. Two datasets closely related to our efforts are SEN12MS [13] and SeCo [4].



Fig. 2. Geographical distribution of SSL4EO-S12 dataset.

However, SEN12MS is limited by geospatial and temporal coverage, SeCo includes optical data, only, and both datasets contain strongly overlapping patches which may negatively impact contrastive methods. With the above in mind, our proposed SSL4EO-S12 dataset provides an improved spatio-temporal coverage by sampling more locations and removing overlapping patches, enclosing multiple seasons, and including Sentinel-1 as well as two Sentinel-2 products embracing two sensor modalities and two popular choices of data products (Table I).

III. SSL4EO-S12 DATASET

A. Data curation & assembly

The SSL4EO-S12 dataset (Figure 1) exploits openly available SAR/optical satellite data collected by the European Space Agency’s Sentinel mission. Following a well-organized baseline provided by SeCo [4], we utilize the Google Earth Engine [24] to download and process the data. We filter image patches to retrieve from the 10,000 most populated cities¹ in the world (top-10k) to guarantee reasonable global coverage. To obtain diverse land cover, we sample 251,079 locations

¹<https://simplemaps.com/data/world-cities>

TABLE I
SUMMARY OF POPULAR PRE-TRAINING DATASETS IN REMOTE SENSING.

dataset	spatial cover	temporal cover	modality	overlap	patch scale
BigEarthNet \cite{sumbul2019bigearthnet}	Europe	1 timestamp	SAR/optical	no	1.2M 120x120
SEN12MS \cite{Schmitt2019}	global	1 timestamp	SAR/optical	yes	540K 256x256
SeCo \cite{manas2021seasonal}	global	5 timestamps	optical	yes	1M 264x264
SSL4EO-S12	global	4 timestamps	SAR/optical	no*	3M 264x264

*Note: our sampling strategy may allow for minor, insignificant patch overlap as detailed in Section III-A, paragraph *Data filtering* and Figure 3.

close by the cities following a Gaussian distribution peaking at the city center and standard deviation of 50km—assuming most of the variability cast to the downtown and suburbs of cities [4]. At each location, we downloaded 4 images drawn from four annual seasons separated by approximately 3 months to capture seasonal variation over the course of a year. We dropped Sentinel-2 tiles with a cloud coverage exceeding 10%—radar based Sentinel-1 images are little affected by clouds. We also filter out most overlapping patches with an efficient grid search strategy. In total, we obtain about one million S1-GRD/S2-L1C/S2-L2A image triplets.

Data identification. The workflow for data collection works as follows:

- 1) Uniformly sample one city from the top-10k populated cities in the world;
- 2) Sample a patch center location from a Gaussian distribution with a standard deviation of 50km around the city center;
- 3) Check if a 2640x2640m image patch (264x264 pixels) centered around that location has significant overlap with previous patches. If this is not the case, continue to 4, otherwise return to 1;
- 4) For a 30-days temporal interval centered at four reference dates (Mar 20, Jun 21, Sep 22, Dec 21) in 2021 (additionally look for 2020 as a buffer), check if there exist Sentinel-2 tiles with less than 10% of cloud coverage (for both L1C and L2A) and corresponding Sentinel-1 GRD product (VV and VH channels) tiles overlapping the randomly sampled, 264x264 pixels patch;
- 5) If there exists valid Sentinel-1/2 tiles close to all the four dates, then process and download all Sentinel-1/2 product tiles into curated image patches, otherwise return to 1.

Data filtering. A simple way to check significant overlap between two patches is to calculate the distance between the two centers. If the distance is smaller than 3/4 the width of a patch, there is a non-negligible overlap. Naively, we need to execute this computation for every new patch relative to all existing patches. However, this becomes inefficient when the number of patches grows large, 250k+ for us. Therefore, we employ a grid search strategy to perform efficient overlap filtering. Instead of calculating the distance to all previous patches, we distribute the patch center coordinates into 360x180 geographical longitude-latitude, one-by-one-degree grids. For each new patch, we convert the center coordinates into integer grid coordinates. Subsequently, we search for existing patches within this grid cell and exclusively calculate distances to those local patches. Assuming potential overlap of sampled patches from distinct grid cells is statistically negligible, we significantly reduce computing resources compared to

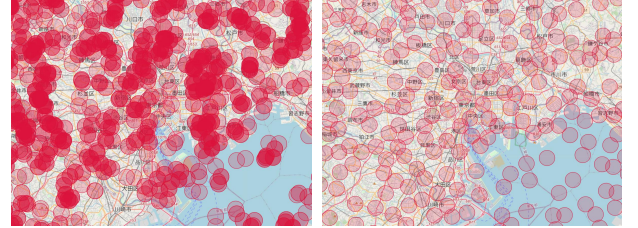


Fig. 3. Image patches without (left) and with (right) overlap filtering in Tokyo metropolitan area. We plot red circles of radius 1.32km (132 pixels) for visualization.

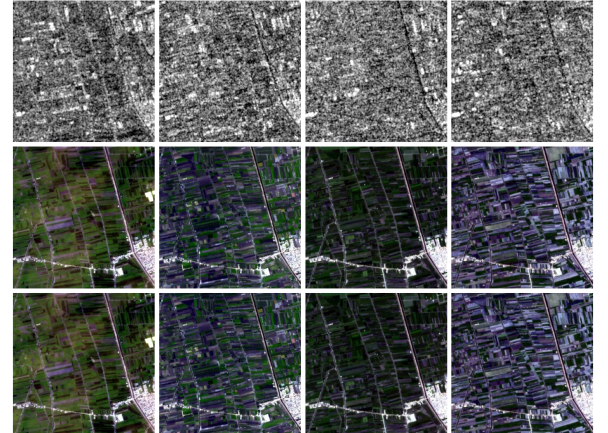


Fig. 4. Sample visualization of one patch from SSL4EO-S12 dataset. The rows top-down present grayscale and false-color imagery based on the Sentinel-1 GRD product, Sentinel-2 level-1C, and Sentinel-2 level-2A multispectral data with corresponding columns representing the four seasons spring, summer, fall, and winter from left to right.

a global overlap search. Indeed, for SSL4EO-S12 we record a tile overlap exceeding 1/4 for approx. 3% of densely populated Tokyo, 1.5% in Chicago, and below 1% for locations such as Beijing, Munich, Kampala, and Brasilia.

B. Data characteristics & volume

The presented SSL4EO-S12 dataset contains 251,079 globally distributed Sentinel-1 dual-pol SAR, Sentinel-2 top-of-atmosphere multispectral, and Sentinel-2 surface reflectance multispectral triplets over four seasonal timestamps. As of summer 2022, SSL4EO-S12 constitutes the biggest geospatial-temporal, multimodal dataset in terms of medium-resolution PolSAR pseudo-imagery and multi-spectral imagery serving more than 3 million such images. The total data volume equates to an uncompressed size of $251,079 \times 4 \times [2 \cdot 4B + (13 + 12) \cdot 2B] \times 264^2 \approx 3.7TB$. Figure 2 depicts the geospatial distribution of the SSL4EO-S12 dataset, highlighting the dense global coverage across the globe. Figure 3

depicts the effect of overlap filtering around Tokyo area. Figure 4 depicts sample patches demonstrating the diversity across various land covers. For bookkeeping, we compute mean and standard deviation of each band’s pixel values for each product, cf. Section VIII.

IV. EXPERIMENTAL SETUP

We evaluate the potential of our proposed SSL4EO-S12 dataset by pre-training and subsequent transfer learning on several downstream tasks.

A. Self-supervised pre-training

We perform pre-training using four well-established self-supervised methodologies, each representing one popular type in self-supervision:

- *MoCo* [14], including its successors MoCo-v2 [25] and MoCo-v3. [26], is a staple contrastive method with explicit negative samples optimizing the InfoNCE loss [27].
- *DINO* [15] employs knowledge distillation without explicit negative sampling.
- *MAE* [16] is a masked autoencoding design by reconstructing missing patches in images.
- *data2vec* [17] follows a recent method that generalizes to various modalities by reconstructing hidden representations of the masked parts instead of raw inputs.

We pre-train ResNet [28] backbones with MoCo(-v2) and DINO, and Vision Transformer (ViT) [29] backbones for all four self-supervised methods listed above. While pre-training in Section V is dominantly running on Sentinel-2 level-1C imagery, additional results for multi-modal training presents Section VI. To utilize multi-temporal information, we use RandomSeasonContrast as a data augmentation strategy, i.e., for MoCo and DINO, the input views are randomly picked from two seasons. For MAE and data2vec, one random season is assigned for each patch in every epoch. We execute training for 100 epochs.

B. Transfer learning

The pre-trained models are transferred to various downstream tasks for evaluation on scene classification and semantic segmentation. For

- *scene classification* we include EuroSAT [30] (single-label land cover classification), BigEarthNet [12] (multi-label land cover classification), and So2Sat-LCZ42 [31] (single-label, local climate zone classification, the culture-10 version).
- *semantic segmentation* we include DFC2020 [32] (land cover segmentation) and OSCD [33] (pixel-wise change detection).

We perform linear probing (freezing the pre-trained encoder parameters) and fine-tuning for the downstream tasks, because 1) linear classification with frozen encoder is a standard evaluation protocol in self-supervised learning thanks to its simplicity and ease of use, and 2) fine-tuning is the most straightforward way to evaluate the upper limit of pre-trained models. Below, we report results in percentage scores for corresponding accuracy metrics.

C. Implementation details

Specifics and additional experimental results for pre-training and transfer learning are provided in Section VIII. Pre-training one ResNet/ViT model for 100 epochs takes 7–25 hours simultaneously running on 4 NVIDIA A100 GPUs, as shown in Table II. In total our experiments consumed more than 1,500 GPU hours.

TABLE II
TRAINING TIME OF THE STUDIED SSL METHODS FOR 100 EPOCHS ON 4 NVIDIA A100 GPUs.

	MoCo	DINO	MAE	data2vec
ResNet50	18h	25h	-	-
ViT-S/16	24h	25h	7h	14h

V. BENCHMARK RESULTS

A. Classification

1) *Comparison of SSL methods*: We first benchmark and evaluate different self-supervised learning methods through linear probing on EuroSAT, BigEarthNet, and So2Sat-LCZ42. As detailed in Table III, all methods outperform random initialization (`rand.init.`) by a substantial margin of order of 10% and more across all datasets. As expected, linear probing on BigEarthNet with all labels performs worse than fully *supervised* training. Promisingly, the gap stays below 5%. On small datasets like BigEarthNet with 10% labels or EuroSAT, linear probing provides results comparable to supervised training within approx. $\pm 1\%$. The trends are slightly different for So2Sat-LCZ42, where the training and testing sets are built upon different cities with a challenging geographical split. Because of this significant domain shift, adding labeled training data does not necessarily improve the testing performance. In fact, fitting the training data distribution does not guarantee out-of-distribution generalization. Nevertheless, the best pre-trained models with linear probing beat the supervised baseline by at least 1% up to about 4%—regardless of the percentage of labels and backbone we did run our experiments on.

On the other hand, all self-supervised learning methods outperform supervised learning with a margin from approx. 1% up to about 6% when fine-tuning the backbone. Top SSL-models score 99.1% on EuroSAT (MoCo/DINO) and over 90% on BigEarthNet (MoCo/DINO) as depicted in Table IV. We note: while fine-tuned models have an edge over supervision depending on dataset and backbone, in linear probing contrastive methods (MoCo and DINO) consistently score better than their image-masking methods (MAE and data2vec) counterparts.

2) *Comparison of different pre-training datasets*: To benchmark our dataset relative to other datasets in (geospatial) computer vision, namely: ImageNet, BigEarthNet, and SeCo, we report corresponding linear probing results pre-trained with MoCo-v2 (ResNet50 backbone) in Table V. For fair comparison we pre-train using RGB bands to reference results reported in SeCo [4]. SSL4EO-S12 significantly outperforms the ImageNet baseline by about 10%. This margin shrinks down to about 1.5%–3.5% utilizing the SeCo dataset with

TABLE III

LINEAR PROBING RESULTS FOR EUROSAT, BIGEARTHNET (BE) WITH 10% AND 100% LABELS, AND SO2SAT-LCZ42 (10% AND 100% LABELS). WE REPORT OVERALL ACCURACY FOR EUROSAT AND SO2SAT-LCZ42, AND MEAN AVERAGE PRECISION FOR BIGEARTHNET. TWO BACKBONE NETWORKS GET TRAINED: RESNET-50 (RN50) AND A SMALL(-S) EMBEDDING DIMENSION VISION TRANSFORMER(VIT) SUBDIVIDING INPUT PATCHES INTO 16X16 TILES(/16). **BOLD** VALUES INDICATE BEST PER-COLUMN PERFORMANCE.

downstream dataset model \ backbone	EuroSAT		BE-10%		BE-100%		So2Sat-10%		So2Sat-100%	
	RN50	ViT-S/16								
rand.init.	82.0	81.3	61.0	60.0	60.0	60.0	48.8	49.3	49.0	50.2
MoCo	98.0	97.7	82.1	82.3	84.2	83.1	61.3	59.6	61.8	62.2
DINO	97.2	97.7	82.0	81.7	83.9	83.4	55.5	60.9	57.0	62.5
MAE	-	94.1	-	77.5	-	78.2	-	59.5	-	60.0
data2vec	-	96.9	-	77.3	-	79.4	-	58.2	-	59.7
supervised	98.0	96.7	83.4	81.3	88.7	87.4	57.5	59.7	57.5	59.3

TABLE IV

FINE-TUNING RESULTS FOR EUROSAT, BIGEARTHNET, AND SO2SAT-LCZ42. ALL BEATING *supervised* TRAINING, CF. TABLE III.

downstream dataset model \ backbone	EuroSAT		BE-10%		BE-100%		So2Sat-10%		So2Sat-100%	
	RN50	ViT-S/16								
MoCo	99.1	98.6	86.2	86.1	91.8	89.9	60.4	61.2	60.9	61.6
DINO	99.1	99.0	87.1	86.9	90.7	90.5	63.2	61.5	63.6	62.2
MAE	-	98.7	-	84.8	-	88.9	-	60.8	-	63.9
data2vec	-	99.1	-	85.6	-	90.3	-	63.2	-	64.8

TABLE V

COMPARISON OF DIFFERENT PRE-TRAINING DATASETS UNDER LINEAR PROBING EVALUATION. "MoCo-v2+TP" REFERS TO PRE-TRAINING WITH MoCo-v2 AND TEMPORAL PAIRS (I.E., *RandomSeasonContrast*) AS REPORTED IN [4]. ALL PERFORMANCE METRICS CITED FROM EXISTING LITERATURE IS MARKED *italic*.

dataset (channels, improved model)	EuroSAT	BE-10%	BE-100%	So2Sat-10%	So2Sat-100%
<i>ImageNet (RGB)</i>	86.4	70.5	71.8	-	-
<i>SeCo (RGB, MoCo-v2+TP)</i>	89.5	74.5	76.3	-	-
<i>SeCo (RGB, multi-subspace)</i>	93.1	78.6	80.4	-	-
<i>SSL4EO-S12 (RGB)</i>	96.6	80.1	82.3	-	-
BigEarthNet (all bands)	94.4	80.6	83.9	53.2	53.6
<i>SSL4EO-S12 (all bands)</i>	98.0	82.1	84.2	61.3	61.8

TABLE VI

COMPARISON OF DIFFERENT PRE-TRAINING DATASETS UNDER FINE-TUNING EVALUATION.

dataset (channels, improved model)	EuroSAT	BE-10%	BE-100%	So2Sat-10%	So2Sat-100%
<i>ImageNet (RGB)</i>	96.5	80.0	86.7	-	-
<i>SeCo (RGB, MoCo-v2+TP)</i>	-	80.2	86.1	-	-
<i>SeCo (RGB, multi-subspace)</i>	97.2	82.6	87.8	-	-
<i>SSL4EO-S12 (RGB)</i>	98.0	82.7	90.9	-	-
BigEarthNet (all bands)	98.9	85.5	89.3	53.0	53.0
<i>SSL4EO-S12 (all bands)</i>	99.1	86.2	91.8	60.4	60.9

MoCo-v2 and its corresponding algorithmic refinements such as *RandomSeasonContrast* or additional *multi-subspace* embedding. Nevertheless, SSL4EO-S12 with plain MoCo-v2 stays superior.

In a second set of experiments we pre-train with MoCo-v2 employing all Sentinel-2 level-1C bands of SSL4EO-S12 and BigEarthNet, respectively. Subsequently, we evaluate performance on all three classification datasets. Results indicate some mild improvements in the range from sub-percentage to about 3.5% for downstream classification based on BigEarthNet. However, the results on EuroSAT and So2Sat-LCZ42 show significant improvements of about 8% when using SSL4EO-S12 over BigEarthNet for pretraining; a hallmark of the SSL4EO-S12 data's capacity to generate generalizable and transferrable models.

Since the above conclusion was based on linear probing, we did iterate our experiments with fine-tuning. Table VI reports corresponding results with consistent trends, but slightly higher absolute accuracy. A difference most notable is ImageNet's catch-up in performance compared to the other

geospatial pre-training datasets. However, a $\sim 5\%$ margin when compared to SSL4EO-S12 persists. The observed is a characteristic feature of the data *domain gap*: while pre-training on ImageNet learns good representations, the weights' distribution is shifted towards natural images, which can be further adjusted to remote sensing data with fine-tuning. We note that fine-tuning is more computationally expensive compared to linear probing, and irrespective of, Tables V and VI demonstrate: pre-training on SSL4EO-S12 does outperform all other datasets for downstream classification.

3) *Comparison of different amounts of labels:* Figure 5 visualizes performance results of transfer learning on BigEarthNet with a varying fraction of labeled samples. Compared to the supervised baseline, self-supervised pre-training on SSL4EO-S12 provides significant benefits when the amount of labeled samples is limited. In fact, fine-tuning on 10% of the labels outperforms the 50%-labels supervised training scenario; and with ViT-S/16, fine-tuning on 50% of the labels outperforms 100%-labels supervised training.

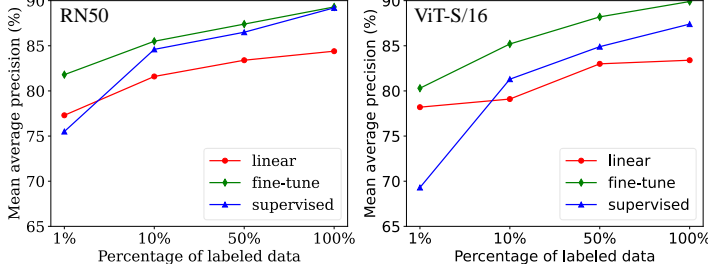


Fig. 5. BigEarthNet (BE) performance depending on amount of labels available to train downstream task. We report linear probing and fine-tuning results pre-trained on MoCo-v2 and backbones ResNet-50 (RN50, left plot) and ViT-S/16 (right plot), respectively.

B. Segmentation

1) *Land cover segmentation*: We use the DFC2020 [32] dataset for the evaluation of land cover semantic segmentation and pre-train a ResNet50 with MoCo-v2 on our SSL4EO-S12 dataset for transfer to the downstream segmentation task. We use PSPNet [34] as segmentation model, and compare the results to random initialization and ImageNet pre-training. Table VII lists results with notable improvements in average accuracy (AA) and mean Intersection-over-Union (mIoU) when compared to ImageNet pre-training. However, SSL4EO-S12 performs worse than ImageNet in overall accuracy (OA). An indicator verifying the excellent visual representation quality of ImageNet pre-training. Future work have to fill this gap for self-supervision by continued methodological development in pixel-based representation learning to better fit segmentation tasks.

2) *Change detection*: In addition to land cover segmentation, we evaluate the pre-trained models for a change detection task on the OSCD [33] dataset. We pre-train a ResNet18 with MoCo-v2 on SSL4EO-S12, and transfer the frozen encoder to the downstream segmentation task. We utilize a U-Net [35] as segmentation model and compare the results with random initialization (`rand.init.`), ImageNet pre-training, and SeCo [4] pre-training. As Table VIII indicates, models pre-trained on SSL4EO-S12 yield superior performance in recall r and F1-score f when referenced to SeCo and ImageNet. As obvious from Table VII, SSL4EO-S12 performs worse in terms of precision p . In fact, random initializing results in the best precision. OSCD is a pixelwise binary change detection

task where most pixels indicate “unchanged” (0) for which the most naive model setting, all pixels to 0, infers a precision score misleading. Hence, the F1-score as a harmonic mean of precision and recall provides an appropriate measure according to $1/f = (1/r + 1/p)/2$.

VI. ADDITIONAL STUDIES

We complete our benchmark by reporting a set of additional studies to document key characteristics of the SSL4EO-S12 dataset, namely: multi-temporal, multimodal, multi-product-level, and data scale.

A. Ablation studies

1) *Benefits of multimodality*: While Section V predominantly employs Sentinel-2 optical data for fair comparison to existing literature, now we highlight the benefits of multimodal self-supervised pre-training with additional Sentinel-1 SAR data. We integrate SAR data following a very simple strategy, using RandomSensorDrop [36] as an additional data augmentation strategy. A ResNet50 is trained with MoCo-v2 on SSL4EO-S12 utilizing optical (S2-L1C) and radar (S1-GRD) products. During training, the model gets fed random combinations of SAR/optical patches, thus learning both inner- and inter-modality representations. Then, the pre-trained model gets transferred to different scenarios where either both modalities or a single one is available. We study the impact of pre-training employing both on BigEarthNet by comparing multimodal pre-training (MM) to uni-modal pre-training (S1/2). Table IX presents results with notable improvement of 1%–3% for 100% and 1% label splits. While single-modality pre-training already provides good performance for both Sentinel-2 and Sentinel-1 data, pre-training exploiting both modalities further improves results.

TABLE VII
DFC2020 LAND COVER SEGMENTATION RESULTS.

dataset	OA	AA	mIoU
rand.init.	52.5	45.0	33.0
ImageNet	56.5	48.4	36.5
SSL4EO-S12	55.7	48.5	39.3

TABLE VIII
OSCD CHANGE DETECTION RESULTS ON RGB CHANNELS.

dataset (# pre-train epochs)	precision	recall	F1
rand.init.	70.5	19.2	29.4
ImageNet	70.4	25.1	36.2
SeCo (200)	69.1	29.7	40.1
SSL4EO-S12 (100)	63.9	32.8	41.0
SSL4EO-S12 (200)	66.9	34.8	42.1

TABLE IX
LINEAR PROBING RESULTS OF MULTIMODAL SELF-SUPERVISED LEARNING. MoCo-S1/2 REPRESENTS PRE-TRAINING WITH ONE SINGLE MODALITY, AND MoCo-MM REPRESENTS PRE-TRAINING WITH BOTH MODALITIES.

downstr./ model	BE-100%			BE-1%		
	S1	S2	S1+2	S1	S2	S1+2
MoCo-S1/2	75.9	84.2	–	71.1	75.9	–
MoCo-MM	79.5	85.1	85.2	73.3	76.7	76.8
supervised	77.2	88.7	88.9	66.7	75.7	76.4

2) *Ablation of seasonal information*: We evaluate the effectiveness of multi-temporal information by replacing seasonal *augmentation* (cf. Section IV) by *random* season: same randomly selected season for the two positive views; and *fixed* season: same season for each patch during training. Pre-training a ResNet50 with MoCo-v2 on a 50k subset of SSL4EO-S12 evaluating on BigEarthNet-10% and EuroSAT yields Table X. The benefits of seasonal augmentation become obvious as the gain in brackets indicates.

TABLE X

LINEAR PROBING RESULTS OF MULTI-TEMPORAL ABLATION STUDY.
IMPROVEMENTS IN ACCURACY COMPARED TO THE FIXED SEASON
SCENARIO ARE HIGHLIGHTED IN BRACKETS.

downstr./season	BE-10%	EuroSAT
fixed	75.1	93.1
random	76.7(+1.6)	94.0(+1.1)
augment	77.6(+2.5)	96.2(+3.1)

3) *Atmospheric correction as data augmentation*: The motivation to include Sentinel-2 level-1C and level-2A products in SSL4EO-S12 simply traces back to freedom of choice for corresponding downstream tasks. However, these product levels with or without atmospheric correction may be considered natural data augmentation for self-supervised learning. Accordingly, we did conduct a related ablation study by pre-training a ResNet50 with MoCo-v2 on a 50k SSL4EO-S12 subset utilizing Sentinel-2 L1C, L2A or both (L1C+L2A). Downstream tasks on L2A products (BigEarthNet-10%) and L1C (EuroSAT) serve as reference. Table XI summarizes our findings: 1) models pre-trained on the same product level as the downstream task have a slight edge ($\sim 1\%$) over models trained on the other product level, and 2) pre-training on both modalities generates a notable improvement of up to 4% compared to the scenario pre-train on one modality and downstream on the other.

TABLE XI

LINEAR PROBING RESULTS OF DIFFERENT PRODUCT LEVELS OF SENTINEL-2. VALUES IN BRACKETS INDICATE IMPROVEMENT RELATIVE TO THE DATA MODALITY PERFORMING WORST.

product	BE-10% (L2A)	EuroSAT (L1C)
L1C	74.0	93.1(+1.1)
L2A	75.1(+1.1)	92.0
L1C+L2A	78.0(+4.0)	93.8(+1.8)

4) *Impact of pre-training scale*: An aspect relevant to large-scale data mining in Earth observation is scaling of results with training data volume: It is technically straightforward to add more images to the SSL4EO-S12 dataset, but why do we stop here? One reason concerns computational costs. We believe the current dataset (1M patches for each Sentinel product, GRD, L1C, and L2A) is comparable to the scale of ImageNet. SSL4EO-S12 serves a good baseline in remote sensing for further development. Moreover, as observed by [37], saturating downstream performance kicks in beyond 500k pre-training images on ImageNet with contrastive learning, with 250k images yielding acceptable results with as little as 1-2% loss in model accuracy. We do observe such a trend in our dataset, too. As demonstrated by Table XII, we pre-trained MoCo-v2

on various amounts of data to report linear probing results for BigEarthNet-10%. While 50% of SSL4EO-S12 (500K) or less pre-training data yields significant performance drops, there's little diminishing gaps from 75% (750K) on.

TABLE XII
LINEAR PROBING RESULTS ON BIGEARTHNET-10% FOR VARIOUS SENTINEL-2 L1C PRE-TRAINING DATA SIZES.

data size	100K	250K	500K	750K	1M
accuracy (%)	64	73	78	81	82

B. Additional ablation of different pre-training protocols

1) *Different ImageNet pre-training protocols*: Table XIII shows a comparison of different ImageNet pre-training protocols. We pre-train ResNet50 with MoCo-v2 for self-supervised pre-training, and report fine-tuning results on BigEarthNet. The table shows that ImageNet pre-training provides good representations that can be generalized well to remote sensing images with RGB but not all bands. It can also be seen that when using RGB, self-supervised pre-training on ImageNet can further improve the downstream performance in remote sensing compared to supervised pre-training.

TABLE XIII
SUMMARY OF DIFFERENT IMAGENET PRE-TRAINING PROTOCOLS.

downstr./ pre-train	All optical bands		RGB	
	BE-10%	BE-100%	BE-10%	BE-100%
Supervised	83.4	88.7	69.5	79.0
ImageNet (Sup)	82.5	89.5	80.0	86.7
ImageNet (SSL)	82.5	89.4	81.9	90.8
SSL4EO-S12 (SSL)	86.2	91.8	82.7	90.9

2) *Supervised pre-training on RS datasets*: Table XIV shows a comparison of supervised and unsupervised pre-training on remote sensing datasets. We do supervised pre-training on BigEarthNet and self-supervised pre-training (MoCo-v2, ResNet50) on both BigEarthNet and SSL4EO-S12. We evaluate the pre-trained models on EuroSAT. The results show that self-supervised pre-training outperforms supervised pre-training on remote sensing data.

TABLE XIV
A COMPARISON OF DIFFERENT PRE-TRAINING PROTOCOLS ON REMOTE SENSING DATASETS AND EVALUATED ON EUROSAT.

downstr./ pre-train	Linear probing		Fine-tuning	
	10%	100%	10%	100%
BigEarthNet (Sup)	80.3	89.3	94.2	98.7
BigEarthNet (SSL)	90.7	94.4	96.3	98.9
SSL4EO-S12 (SSL)	92.7	98.0	96.9	99.1

C. Representation visualization

We qualitatively evaluate the data representations learned from self-supervised pre-training by visualizing the latent distributions with T-SNE, Figure 6). We pre-train a ResNet50 with MoCo-v2 on our SSL4EO-S12 dataset, and transfer the frozen encoder to EuroSAT. For each image in EuroSAT, we calculate one 128d representation vector. We then visualize all the vectors with T-SNE (after an intermediate PCA to 50d).

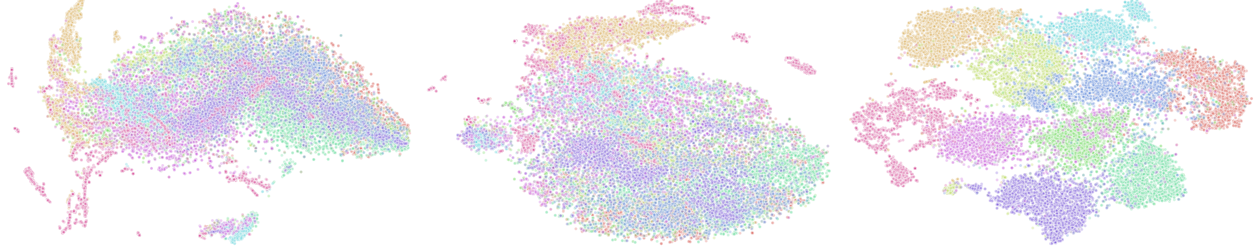


Fig. 6. T-SNE visualization of image representations from EuroSAT (10 classes). From left to right: raw input, random-encoded features, SSL-encoded features. SSL encoded features are well clustered even without label information.

VII. CONCLUSION

In this work, we did present SSL4EO-S12—a large-scale unlabeled dataset for self-supervised learning in Earth observation. By integrating multimodal, multi-temporal and multi-product-level characteristics with global coverage, we do believe SSL4EO-S12 serves as relevant pre-training dataset for remote sensing in Earth observation. Our results support the value of SSL4EO-S12 for a set of popular self-supervised training methods, including relevant downstream tasks for remote sensing applications.

To summarize the diverse set of benchmark experiments carried out in Sections V and VI, a general take-away reads: Given the Earth surface cover related downstream tasks at hand,

- information from the multi-spectral optical channels seem to dominantly contribute to model performance
- SAR-optical fusion marginally helps to improve performance over single-modal optical models, and
- SAR-only downstream applications can benefit from SAR-optical, multimodal pre-training.

However, SSL4EO-S12 leaves potential for future dataset contributions: Although it targets at general Earth observation, SSL4EO-S12 puts focus on human-inhabited lands with little coverage of ocean and polar regions. Moreover, we did employ uniform sampling (from top-10k populated cities) and Gaussian sampling (with radius of 50km from city center) to implement global and diverse land coverage. Yet, bias does exist, e.g. due to additional filtering for clouds. Besides, we employed an efficient grid search strategy to avoid significant overlap within each grid cell. However, the algorithm ignores cell boundaries. Hence, the dataset is not strictly free of geospatial overlap. Lastly, the SSL4EO-S12 does exclusively provide information from medium resolution radar and multi-spectral image modalities—a limited subset of Earth observation data made available by the plurality of remote sensing devices. Despite these limitations, SSL4EO-S12 renders a valuable basis for numerical experiments to advance self-supervised learning and large-scale data mining in remote sensing and Earth observation.

VIII. ETHICAL CONSIDERATIONS

To the degree we are aware of, our work has little to no ethical or social issues of concern. The dataset got assembled from openly available Sentinel-1/2 satellite imagery of years

2020/21 without any human annotations included. The Copernicus Programme is a European initiative where GDPR applies since 2018 [38]. Although all imagery is geo-referenced, each patch is based on a spatial ground sampling distance of no more than 10 meters masking details such as identification of individuals on the ground. Nevertheless, an aspect we note: the limited spatio-temporal sampling rate and associated data availability constraints, such as cloud coverage, may introduce model bias possibly impacting the transfer learning performance for out-of-distribution geographic scenes.

ACKNOWLEDGMENTS

This work was jointly supported by the European Research Council (ERC) under the European Union’s Horizon 2020 research and innovation programme (grant agreement No. [ERC-2016-StG-714087], Acronym: *So2Sat* and grant agreement No. [957407], Acronym: *DAPHNE*), the Helmholtz Association through the Framework of Helmholtz AI (grant number: ZT-IPF-5-01) - Local Unit “Munich Unit @Aeronautics, Space and Transport (MASTr)”, the Helmholtz Klimainitiative (HICAM) and Helmholtz Excellent Professorship “Data Science in Earth Observation - Big Data Fusion for Urban Research” (grant number: W2-W3-100), the German Federal Ministry of Education and Research (BMBF) in the framework of the international future AI lab “AI4EO – Artificial Intelligence for Earth Observation: Reasoning, Uncertainties, Ethics and Beyond” (grant number: 01DD20001), and the German Federal Ministry for Economic Affairs and Climate Action in the framework of the “national center of excellence ML4Earth” (grant number: 50EE2201C). The computing resources were supported by the Helmholtz Association’s Initiative and Networking Fund on the HAICORE@FZJ partition.

REFERENCES

- [1] Xiao Liu et al. “Self-supervised learning: Generative or contrastive”. In: *IEEE Transactions on Knowledge and Data Engineering* (2021) (cit. on p. 1).
- [2] Zhitong Xiong et al. “EarthNets: Empowering AI in Earth Observation”. In: *arXiv preprint arXiv:2210.04936* (2022) (cit. on p. 1).
- [3] Kumar Ayush et al. “Geography-Aware Self-Supervised Learning”. In: *Proceedings of the IEEE/CVF International Conference on Computer Vision (ICCV)*. 2021, pp. 10181–10190 (cit. on p. 1).

[4] Oscar Mañas et al. “Seasonal contrast: Unsupervised pre-training from uncurated remote sensing data”. In: *Proceedings of the IEEE/CVF International Conference on Computer Vision*. 2021, pp. 9414–9423 (cit. on pp. 1–6, 12, 16).

[5] Konrad Heidler et al. “Self-supervised Audiovisual Representation Learning for Remote Sensing Data”. In: *arXiv preprint arXiv:2108.00688* (2021) (cit. on p. 1).

[6] Haifeng Li et al. “Global and local contrastive self-supervised learning for semantic segmentation of HR remote sensing images”. In: *IEEE Transactions on Geoscience and Remote Sensing* 60 (2022), pp. 1–14 (cit. on p. 1).

[7] Sudipan Saha, Patrick Ebel, and Xiao Xiang Zhu. “Self-supervised multisensor change detection”. In: *IEEE Transactions on Geoscience and Remote Sensing* (2021) (cit. on p. 1).

[8] Vladan Stojnic and Vladimir Risojevic. “Self-supervised learning of remote sensing scene representations using contrastive multiview coding”. In: *Proceedings of the IEEE/CVF Conference on Computer Vision and Pattern Recognition*. 2021, pp. 1182–1191 (cit. on p. 1).

[9] Chenchen Wang, Hong Gu, and Weimin Su. “SAR image classification using contrastive learning and pseudo-labels with limited data”. In: *IEEE Geoscience and Remote Sensing Letters* 19 (2021), pp. 1–5 (cit. on p. 1).

[10] Bing Liu et al. “Deep multiview learning for hyperspectral image classification”. In: *IEEE Transactions on Geoscience and Remote Sensing* 59.9 (2020), pp. 7758–7772 (cit. on p. 1).

[11] Jia Deng et al. “Imagenet: A large-scale hierarchical image database”. In: *2009 IEEE conference on computer vision and pattern recognition*. Ieee. 2009, pp. 248–255 (cit. on p. 1).

[12] Gencer Sumbul et al. “Bigearthnet: A large-scale benchmark archive for remote sensing image understanding”. In: *IGARSS 2019-2019 IEEE International Geoscience and Remote Sensing Symposium*. IEEE. 2019, pp. 5901–5904 (cit. on pp. 1, 2, 4, 16).

[13] Michael Schmitt et al. “SEN12MS – a curated dataset of georeferenced multi-spectral Sentinel-1/2 imagery for deep learning and data fusion”. In: *ISPRS Annals of the Photogrammetry, Remote Sensing and Spatial Information Sciences*. Vol. IV-2/W7. 2019, pp. 153–160. DOI: 10.5194/isprs-annals-IV-2-W7-153-2019 (cit. on pp. 1, 2, 16).

[14] Kaiming He et al. “Momentum contrast for unsupervised visual representation learning”. In: *Proceedings of the IEEE/CVF conference on computer vision and pattern recognition*. 2020, pp. 9729–9738 (cit. on pp. 1, 4).

[15] Mathilde Caron et al. “Emerging properties in self-supervised vision transformers”. In: *Proceedings of the IEEE/CVF International Conference on Computer Vision*. 2021, pp. 9650–9660 (cit. on pp. 1, 4).

[16] Kaiming He et al. “Masked autoencoders are scalable vision learners”. In: *arXiv preprint arXiv:2111.06377* (2021) (cit. on pp. 1, 2, 4).

[17] Alexei Baevski et al. “Data2vec: A general framework for self-supervised learning in speech, vision and language”. In: *arXiv preprint arXiv:2202.03555* (2022) (cit. on pp. 1, 2, 4).

[18] Ting Chen et al. “A simple framework for contrastive learning of visual representations”. In: *International conference on machine learning*. PMLR. 2020, pp. 1597–1607 (cit. on p. 1).

[19] Jean-Bastien Grill et al. “Bootstrap your own latent-a new approach to self-supervised learning”. In: *Advances in Neural Information Processing Systems* 33 (2020), pp. 21271–21284 (cit. on p. 1).

[20] Jure Zbontar et al. “Barlow twins: Self-supervised learning via redundancy reduction”. In: *International Conference on Machine Learning*. PMLR. 2021, pp. 12310–12320 (cit. on p. 1).

[21] Mathilde Caron et al. “Unsupervised learning of visual features by contrasting cluster assignments”. In: *Advances in Neural Information Processing Systems* 33 (2020), pp. 9912–9924 (cit. on p. 2).

[22] Jinghao Zhou et al. “ibot: Image bert pre-training with online tokenizer”. In: *arXiv preprint arXiv:2111.07832* (2021) (cit. on p. 2).

[23] Minyoung Huh, Pulkit Agrawal, and Alexei A Efros. “What makes ImageNet good for transfer learning?” In: *arXiv preprint arXiv:1608.08614* (2016) (cit. on p. 2).

[24] Noel Gorelick et al. “Google Earth Engine: Planetary-scale geospatial analysis for everyone”. In: *Remote sensing of Environment* 202 (2017), pp. 18–27 (cit. on pp. 2, 14, 15).

[25] Xinlei Chen et al. “Improved baselines with momentum contrastive learning”. In: *arXiv preprint arXiv:2003.04297* (2020) (cit. on p. 4).

[26] Xinlei Chen, Saining Xie, and Kaiming He. “An empirical study of training self-supervised vision transformers”. In: *Proceedings of the IEEE/CVF International Conference on Computer Vision*. 2021, pp. 9640–9649 (cit. on p. 4).

[27] Aaron Van den Oord, Yazhe Li, and Oriol Vinyals. “Representation learning with contrastive predictive coding”. In: *arXiv e-prints* (2018), arXiv–1807 (cit. on p. 4).

[28] Kaiming He et al. “Deep residual learning for image recognition”. In: *Proceedings of the IEEE conference on computer vision and pattern recognition*. 2016, pp. 770–778 (cit. on p. 4).

[29] Alexey Dosovitskiy et al. “An image is worth 16x16 words: Transformers for image recognition at scale”. In: *arXiv preprint arXiv:2010.11929* (2020) (cit. on p. 4).

[30] Patrick Helber et al. “Eurosat: A novel dataset and deep learning benchmark for land use and land cover classification”. In: *IEEE Journal of Selected Topics in Applied Earth Observations and Remote Sensing* 12.7 (2019), pp. 2217–2226 (cit. on p. 4).

- [31] Xiao Xiang Zhu et al. “So2Sat LCZ42: A benchmark dataset for global local climate zones classification”. In: *arXiv preprint arXiv:1912.12171* (2019) (cit. on p. 4).
- [32] Michael Schmitt et al. *2020 IEEE GRSS Data Fusion Contest*. 2019. DOI: 10.21227/rha7-m332. URL: <https://dx.doi.org/10.21227/rha7-m332> (cit. on pp. 4, 6).
- [33] Rodrigo Caye Daudt et al. “Urban change detection for multispectral earth observation using convolutional neural networks”. In: *IGARSS 2018-2018 IEEE International Geoscience and Remote Sensing Symposium*. IEEE. 2018, pp. 2115–2118 (cit. on pp. 4, 6, 12).
- [34] Hengshuang Zhao et al. “Pyramid scene parsing network”. In: *Proceedings of the IEEE conference on computer vision and pattern recognition*. 2017, pp. 2881–2890 (cit. on p. 6).
- [35] Olaf Ronneberger, Philipp Fischer, and Thomas Brox. “U-net: Convolutional networks for biomedical image segmentation”. In: *International Conference on Medical image computing and computer-assisted intervention*. Springer. 2015, pp. 234–241 (cit. on p. 6).
- [36] Yi Wang, Conrad M Albrecht, and Xiao Xiang Zhu. “Self-supervised Vision Transformers for Joint SAR-optical Representation Learning”. In: *arXiv preprint arXiv:2204.05381* (2022) (cit. on p. 6).
- [37] Elijah Cole et al. “When does contrastive visual representation learning work?” In: *Proceedings of the IEEE/CVF Conference on Computer Vision and Pattern Recognition*. 2022, pp. 14755–14764 (cit. on p. 7).
- [38] *Fact sheet on the protection of personal data in the European Union*. European Parliament. URL: <https://www.europarl.europa.eu/factsheets/en/sheet/157/personal-data-protection> (visited on 08/12/2022) (cit. on p. 8).
- [39] Ramon Torres et al. “GMES Sentinel-1 mission”. In: *Remote sensing of environment* 120 (2012), pp. 9–24 (cit. on p. 11).
- [40] Matthias Drusch et al. “Sentinel-2: ESA’s optical high-resolution mission for GMES operational services”. In: *Remote sensing of Environment* 120 (2012), pp. 25–36 (cit. on p. 11).
- [41] Guangrun Wang et al. “Semantic-Aware Auto-Encoders for Self-Supervised Representation Learning”. In: *Proceedings of the IEEE/CVF Conference on Computer Vision and Pattern Recognition*. 2022, pp. 9664–9675 (cit. on p. 13).
- [42] Zhirong Wu et al. “Extreme Masking for Learning Instance and Distributed Visual Representations”. In: *arXiv preprint arXiv:2206.04667* (2022) (cit. on p. 13).
- [43] Timnit Gebru et al. “Datasheets for datasets”. In: *Communications of the ACM* 64.12 (2021), pp. 86–92 (cit. on p. 16).

APPENDIX

A. Additional information of the dataset

1) *Sentinel-1/2*: The proposed SSL4EO-S12 dataset exploits freely available SAR/optical satellite images from European Space Agency's Sentinel mission (under the CC-BY license).

The Sentinel-1 mission [39] consists of two polar-orbiting satellites, equipped with C-band SAR sensors, which enables them to acquire imagery regardless of the weather. For the Sentinel-1 images in the SSL4EO-S12 dataset, ground-range-detected (GRD) products with both VH and VV polarization acquired in the interferometric wide swath (IW) mode were used. These images contain the σ^0 backscatter coefficient in dB scale. The image resolution is 10m.

The Sentinel-2 mission [40] comprises two polar-orbiting satellites in the same orbit, equipped with multi-spectral imaging sensors. For Sentinel-2 images in the SSL4EO-S12 dataset, both level-1C top-of-atmosphere reflectance (13 bands) and level-2A atmospherically corrected surface reflectance (12 bands) were included. The image resolution ranges between 10m (visible and NIR), 20m (red edge and SWIR) and 60m (aerosols).

2) *Dataset statistics*: Table XV and XVI present the mean and standard deviation of each band for each product of the proposed SSL4EO-S12 dataset.

TABLE XV
STATISTICS OF SENTINEL-1 IMAGES IN THE SSL4EO-S12 DATASET.

	VV	VH
mean	-12.59	-20.26
std	5.26	5.91

TABLE XVI
STATISTICS OF SENTINEL-2 IMAGES IN THE SSL4EO-S12 DATASET.

	B1	B2 (B)	B3 (G)	B4 (R)	B5	B6	B7	B8	B8A	B9	B10	B11	B12	
s2c	mean	1612.9	1397.6	1322.3	1373.1	1561.0	2108.4	2390.7	2318.7	2581.0	837.7	22.0	2195.2	1537.4
	std	791.0	854.3	878.7	1144.9	1127.5	1164.2	1276.0	1249.5	1345.9	577.5	47.5	1340.0	1142.9
s2a	mean	756.4	889.6	1151.7	1307.6	1637.6	2212.6	2442.0	2538.9	2602.9	2666.8	-	2388.8	1821.5
	std	1111.4	1159.1	1188.1	1375.2	1376.6	1358.6	1418.4	1476.4	1439.9	1582.1	-	1460.7	1352.2

3) *Data storage*: The SSL4EO-S12 dataset is stored in GeoTiff format for each band of each patch. The file structure is shown in Figure 7, where s1/s2a/s2c represents Sentinel-1 / Sentinel-2 level-2A / Sentinel-2 level-1C, and t1 - t4 represent 4 seasons. Raw files (extracted GeoTiff) occupy about 500GB/800GB/800GB disk storage for S1/S2A/S2C, and compressed tar.gz files occupy about 450GB/500GB/500GB correspondingly.

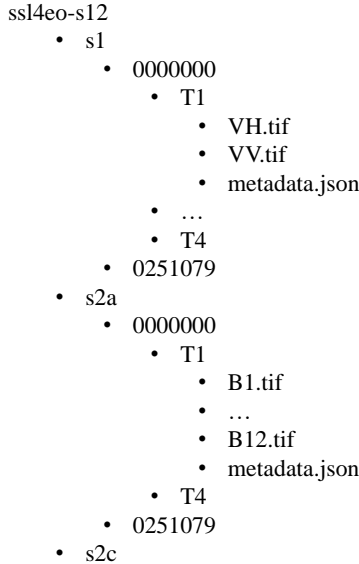


Fig. 7. SSL4EO-S12 file structure.

4) *metadata.json*: Each patch comes with a metadata file that collects the image properties of this patch. See section VIII-D for details.

B. Implementation details

1) *Pre-training*: We use Sentinel-2 level-1C images for the main pre-training experiments, which are pre-processed by converting to uint8 for efficiency (divided by 10000 and multiplied by 255, see Section VIII-C). We use 4 NVIDIA A100 GPUs with a total batch size of 256 for all the pre-training experiments. For the main experiments, we pre-train ResNet50 or ViT-S/16 for 100 epochs. Training time varies between different methods from 7 to 25 hours, as shown in Table II. The total experiments (including parameter tuning) take about 70k core hours (1400 GPU hours).

MoCo. We pre-train the MoCo-v2/v3 models using their default settings following the publicly available repository (<https://github.com/facebookresearch/moco> and <https://github.com/facebookresearch/moco-v3>). We use RandomResizedCrop, RandomBrightness/Contrast (to have a partial color jittering for multiple bands), RandomGrayscale, RandomGaussianBlur, RandomHorizontalFlip and RandomSeasonContrast (see Section IV) as data augmentations. For MoCo-v2 (ResNet50), we use SGD optimizer and cosine learning rate schedule with a learning rate 0.03. For MoCo-v3 (ViT-S/16), we use AdamW optimizer and cosine schedule with a learning rate 1.5e-4.

DINO. We pre-train the DINO models using its default settings following the publicly available repository (<https://github.com/facebookresearch/dino>). The data augmentations include those of MoCo, as well as additional Multi-Crop and Solarization. For ResNet50, we use SGD optimizer and cosine learning rate schedule with a learning rate 0.03. For ViT-S/16, we use AdamW optimizer and cosine learning rate schedule with a learning rate 1.5e-4.

MAE. We pre-train the MAE models using its default settings following the publicly available repository (<https://github.com/facebookresearch/mae>). The mask ratio is set to 0.7. The data augmentations include RandomResizedCrop, RandomHorizontalFlip and RandomSeason. We use AdamW optimizer and cosine learning rate schedule with a learning rate 1.5e-4.

data2vec. We pre-train the data2vec models using its default settings following the publicly available repository (<https://github.com/facebookresearch/fairseq/tree/main/examples/data2vec>). The data augmentations include Resize/CenterCrop, RandomHorizontalFlip and RandomSeason. We use AdamW optimizer and cosine learning rate schedule with a learning rate 1e-3.

2) *Downstream tasks*: Below are implementation details for the downstream tasks.

EuroSAT. We split EuroSAT into 21600 training and 5400 testing images for evaluation. The data augmentations are RandomResizedCrop/RandomHorizontalFlip for training, and Resize/CenterCrop for testing. We resize the images to 224x224 for better performance (see Section VIII-C). The batch size is 256. We use CrossEntropyLoss and SGD optimizer with step decay learning rate (divided by 10 at epoch 60 and 80) for 100 epochs. We use simple grid search strategy to find suitable learning rates for linear probing and fine-tuning.

BigEarthNet. We use 311667 training and 103944 testing images from BigEarthNet for evaluation. Different settings of amount of labels affect only the training split. The data augmentations are RandomResizedCrop/RandomHorizontalFlip for training, and Resize/CenterCrop for testing. We use a cropping scale of 0.8 to avoid strong occlusions (BigEarthNet is a multi-label dataset). We resize the images to 224x224 for better performance. The batch size is 256. We use MultiLabelSoftMarginLoss and SGD optimizer with step decay learning rate (divided by 10 at epoch 60 and 80) for 100 epochs. We use simple grid search strategy to find suitable learning rates for linear probing and fine-tuning.

So2Sat-LCZ42. We use 352366 training and 24119 testing Sentinel-2 images from So2Sat-LCZ42 for evaluation. Different settings of amount of labels affect only the training split. We use the *culture-10* version of So2Sat-LCZ42: the training data and the testing data are from different cities. The data augmentations are RandomResizedCrop/RandomHorizontalFlip for training, and Resize/CenterCrop for testing. We resize the images to 224x224 for better performance. The batch size is 256. We use CrossEntropyLoss and SGD optimizer with step decay learning rate (divided by 10 at epoch 60 and 80) for 100 epochs. We use simple grid search strategy to find suitable learning rates for linear probing and fine-tuning.

DFC2020. We use 5128 training and 986 testing Sentinel-2 images from DFC2020 dataset for evaluation. The batch size is set to 8 and we train the models for 100 epochs. We use CrossEntropyLoss and SGD optimizer with momentum 0.9 and weight decay 5e-4. The initial learning rate is 1e-3, which is decayed by a factor of 0.9 in every epoch until 1e-4.

OSCD. This dataset is composed of 24 pairs of multispectral images from Sentinel-2 in total. Following [33], we use 14 of them for training, and the rest for testing. In fine-tuning stage, we adopt settings similar to those in [4]. That is, the original images are split into non-overlapping patches of 96×96 pixels as inputs, which leads to 827 and 285 patches for training and test, respectively. The batch size is set to 32. In terms of optimizer, we use Adam with a weight decay of 1e-4. The initial learning rate is 5e-3, and decreases exponentially with a multiplicative factor of 0.95 for every epoch. The resulting models are evaluated on the test set after 100 epochs.

C. Additional experimental results

1) *Data pre-processing*: We show the influence of data pre-processing (for pre-training) in Table XVII, where int16 means 16 bits raw input, uint8 means compressed 8 bits input (divided by 10000 and multiplied by 255), uint8-n means normalization by mean and standard deviation, and L2A/L1C means with/without atmospheric correction. The results show similar performance between 16 bit and 8 bit, supporting compressed input as it saves a lot of storage space and computing time. The results also

show comparable performance for L1C and L2A, as well as for the use of normalization. Therefore, in our main experiments, we use level-1C, uint8, unnormalized data for pre-training.

TABLE XVII

EFFECTS OF PRE-PROCESSING FOR PRE-PRETRAINING. WE PRE-TRAIN A RESNET50 WITH MoCo-v2 ON A 50K SUBSET FOR EFFICIENCY AND REPORT LINEAR PROBING RESULTS.

	BE-10% (L2A)			EuroSAT (L1C)		
	int16	uint8	uint8-n	int16	uint8	uint8-n
L2A	73.9	73.9	75.6	85.2	86.6	-
L1C	73.8	74	-	86.2	87.7	85.1

2) *Downstream input size*: We analyze the impact of image resolution on pre-training and transfer learning in Table XVIII. We clearly observe the advantage of upsampling the input image size. Therefore, in our main experiments, we upscale the downstream input images to 224x224 for better performance.

TABLE XVIII

EFFECTS OF INPUT SIZE OF DOWNSTREAM TASKS. WE PRE-TRAIN RESNET50 WITH MoCo-v2 ON THE 50K SUBSET FOR EFFICIENCY AND REPORT LINEAR PROBING RESULTS.

	BE-10%			EuroSAT		
	224	112	56	224	112	56
pretrain 224	75.1	71.1	-	93.1	89.4	89.4
pretrain 112	75.9	73.9	-	92.7	91.1	86.6
pretrain 56	73.1	70.5	70.5	89.7	89	86.4

3) *Masking ratios of MAE*: Table XIX shows the influence of masking ratios in MAE during pre-training. We find 70% to be the best masking ratio, which is similar to natural images as reported in MAE paper, where 75% is the best. It is also promising to see that the model still learns good representations even with 90% pixels masked. However, in general MAE is performing worse than other SSL methods on linear probing (see Table III), which has also been reported in recent works [41, 42].

TABLE XIX

EFFECTS OF DIFFERENT MASKING RATIOS. WE PRE-TRAIN ViT-S/16 WITH MAE ON THE 50K SUBSET FOR EFFICIENCY AND REPORT LINEAR PROBING RESULTS ON BIGEARTHNET-10%.

Mask ratio	90%	80%	75%	70%	60%	50%
BE-10%	72	73.5	73.8	74	73.6	72.9

4) *Multispectral results on OSCD dataset*: Table XX shows the results of using all 13 bands for change detection. We pre-train ResNet18 with MoCo-v2 for 100 epochs.

TABLE XX
ADDITIONAL 13-BAND RESULTS ON OSCD DATASET.

	precision	recall	F1
Random	55.60	24.09	31.25
SSL4EO-S12	64.78	33.29	41.85

D. Metadata

See table XXII and XXI for a list of metadata in *meta.json*.

TABLE XXI
METADATA SENTINEL-1[24].

Name	Type	Description
GRD_Post_Processing_facility_country	STRING	Name of the country where the facility is located. This element is configurable within the IPF.
GRD_Post_Processing_facility_name	STRING	Name of the facility where the processing step was performed. This element is configurable within the IPF.
GRD_Post_Processing_facility_organisation	STRING	Name of the organisation responsible for the facility. This element is configurable within the IPF.
GRD_Post_Processing_facility_site	STRING	Geographical location of the facility. This element is configurable within the IPF.
GRD_Post_Processing_software_name	STRING	Name of the software.
GRD_Post_Processing_software_version	STRING	Software version identification.
GRD_Post_Processing_start	DOUBLE	Processing start time.
GRD_Post_Processing_stop	DOUBLE	Processing stop time.
SLC_Processing_facility_country	STRING	Name of the country where the facility is located. This element is configurable within the IPF.
SLC_Processing_facility_name	STRING	Name of the facility where the processing step was performed. This element is configurable within the IPF.
SLC_Processing_facility_organisation	STRING	Name of the organisation responsible for the facility. This element is configurable within the IPF.
SLC_Processing_facility_site	STRING	Geographical location of the facility. This element is configurable within the IPF.
SLC_Processing_software_name	STRING	Name of the software.
SLC_Processing_software_version	STRING	Software version identification.
SLC_Processing_start	DOUBLE	Processing start time.
SLC_Processing_stop	DOUBLE	Processing stop time.
S1TBX_Calibration_Operator_version	STRING	Sentinel-1 Toolbox calibration tool version.
S1TBX_SAR_Processing_version	STRING	Sentinel-1 Toolbox SAR processing tool version.
SNAP_Graph_Processing_Framework_GPF_version	STRING	Sentinel Application Platform (SNAP) version.
startTimeANX	DOUBLE	Sensing start time of the input data relative to the ascending node crossing. This is a count of the time elapsed since the orbit ascending node crossing [ms].
stopTimeANX	DOUBLE	Sensing stop time of the input data relative to the ascending node crossing. This is a count of the time elapsed since the orbit ascending node crossing [ms].
nssdcIdentifier	STRING	Uniquely identifies the mission according to standards defined by the World Data Center for Satellite Information (WDC-SI), available here.
familyName	STRING	The full mission name. E.g. "SENTINEL-1"
platform_number	STRING	The alphanumeric identifier of the platform within the mission.
instrument	STRING	Information related to the instrument on the platform to which acquired the data.
instrumentMode	STRING	IW (Interferometric Wide Swath), EW (Extra Wide Swath) or SM (Strip Map)
instrumentSwath	STRING	List of the swaths contained within a product. Most products will contain only one swath, except for TOPS SLC products which include 3 or 5 swaths.
orbitNumber_start	DOUBLE	Absolute orbit number of the oldest line within the image data.
orbitNumber_stop	DOUBLE	Absolute orbit number of the most recent line within the image data.
relativeOrbitNumber_start	DOUBLE	Relative orbit number of the oldest line within the image data.
relativeOrbitNumber_stop	DOUBLE	Relative orbit number of the most recent line within the image data.
cycleNumber	DOUBLE	Absolute sequence number of the mission cycle to which the oldest image data applies.
phaseIdentifier	DOUBLE	Id of the mission phase to which the oldest image data applies.
orbitProperties_pass	STRING	Direction of the orbit ('ASCENDING' or 'DESCENDING') for the oldest image data in the product (the start of the product).
orbitPropertiesAscendingNodeTime	DOUBLE	UTC time of the ascending node of the orbit. This element is present for all products except ASAR L2 OCN products which are generated from an ASAR L1 input.
resolution	STRING	H for high or M for medium.
resolution_meters	DOUBLE	Resolution in meters.
instrumentConfigurationID	DOUBLE	The instrument configuration ID (Radar database ID) for this data.
missionDataTakeID	DOUBLE	Unique ID of the data take within the mission.
transmitterReceiverPolarisation	DOUBLE	Transmit/Receive polarisation for the data. There is one element for each Tx/Rx combination: ["VV"], ["HH"], ["VH"], ["HV"], or ["HH", "HV"].
productClass	STRING	Output product class "A" for Annotation or "S" for Standard.
productClassDescription	STRING	Textual description of the output product class.
productComposition	STRING	The composition type of this product: "Individual", "Slice", or "Assembled".
productType	STRING	The product type (correction level) of this product.
productTimelinessCategory	STRING	Describes the required timeliness of the processing. One of: NRT-10m, NRT-1h, NRT-3h, Fast-24h, Off-line, or Reprocessing
sliceProductFlag	STRING	True if this is a slice from a larger product or false if this is a complete product.
segmentStartTime	DOUBLE	Sensing start time of the segment to which this slice belongs. This field is only present if sliceProductFlag = true
sliceNumber	DOUBLE	Absolute slice number of this slice starting at 1. This field is only present if sliceProductFlag = true.
totalSlices	DOUBLE	Total number of slices in the complete data take. This field is only present if sliceProductFlag = true.

TABLE XXII
METADATA SENTINEL-2[24].

Name	Type	Description
AOT_RETRIEVAL_ACCURACY	DOUBLE	Accuracy of Aerosol Optical thickness model
CLOUDY_PIXEL_PERCENTAGE	DOUBLE	Granule-specific cloudy pixel percentage taken from the original metadata
CLOUD_COVERAGE_ASSESSMENT	DOUBLE	Cloudy pixel percentage for the whole archive that contains this granule. Taken from the original metadata
CLOUDY_SHADOW_PERCENTAGE	DOUBLE	Percentage of pixels classified as cloud shadow
DARK_FEATURES_PERCENTAGE	DOUBLE	Percentage of pixels classified as dark features or shadows
DATASTRIP_ID	STRING	Unique identifier of the datastrip Product Data Item (PDI)
DATATAKE_IDENTIFIER	STRING	Uniquely identifies a given Datatake. The ID contains the Sentinel-2 satellite, start date and time, absolute orbit number, and processing baseline.
DATATAKE_TYPE	STRING	MSI operation mode
DEGRADED_MS1_DATA_PERCENTAGE	DOUBLE	Percentage of degraded MSI and ancillary data
FORMAT_CORRECTNESS	STRING	Synthesis of the On-Line Quality Control (OLQC) checks performed at granule (Product_Syntax) and datastrip (Product_Syntax and DS_Conistency) levels
GENERAL_QUALITY	STRING	Synthesis of the OLQC checks performed at the datastrip level (Relative_Orbit_Number)
GENERATION_TIME	DOUBLE	Product generation time
GEOMETRIC_QUALITY	STRING	Synthesis of the OLQC checks performed at the datastrip level (Attitude_Quality_Indicator)
GRANULE_ID	STRING	Unique identifier of the granule PDI (PDI_ID)
HIGH_PROBA_CLOUDS_PERCENTAGE	DOUBLE	Percentage of pixels classified as high probability clouds
MEAN_INCIDENCE_AZIMUTH_ANGLE_B1	DOUBLE	Mean value containing viewing incidence azimuth angle average for band B1 and for all detectors
MEAN_INCIDENCE_AZIMUTH_ANGLE_B2	DOUBLE	Mean value containing viewing incidence azimuth angle average for band B2 and for all detectors
MEAN_INCIDENCE_AZIMUTH_ANGLE_B3	DOUBLE	Mean value containing viewing incidence azimuth angle average for band B3 and for all detectors
MEAN_INCIDENCE_AZIMUTH_ANGLE_B4	DOUBLE	Mean value containing viewing incidence azimuth angle average for band B4 and for all detectors
MEAN_INCIDENCE_AZIMUTH_ANGLE_B5	DOUBLE	Mean value containing viewing incidence azimuth angle average for band B5 and for all detectors
MEAN_INCIDENCE_AZIMUTH_ANGLE_B6	DOUBLE	Mean value containing viewing incidence azimuth angle average for band B6 and for all detectors
MEAN_INCIDENCE_AZIMUTH_ANGLE_B7	DOUBLE	Mean value containing viewing incidence azimuth angle average for band B7 and for all detectors
MEAN_INCIDENCE_AZIMUTH_ANGLE_B8	DOUBLE	Mean value containing viewing incidence azimuth angle average for band B8 and for all detectors
MEAN_INCIDENCE_AZIMUTH_ANGLE_B8A	DOUBLE	Mean value containing viewing incidence azimuth angle average for band B8a and for all detectors
MEAN_INCIDENCE_AZIMUTH_ANGLE_B9	DOUBLE	Mean value containing viewing incidence azimuth angle average for band B9 and for all detectors
MEAN_INCIDENCE_AZIMUTH_ANGLE_B10	DOUBLE	Mean value containing viewing incidence azimuth angle average for band B10 and for all detectors
MEAN_INCIDENCE_AZIMUTH_ANGLE_B11	DOUBLE	Mean value containing viewing incidence azimuth angle average for band B11 and for all detectors
MEAN_INCIDENCE_AZIMUTH_ANGLE_B12	DOUBLE	Mean value containing viewing incidence azimuth angle average for band B12 and for all detectors
MEAN_INCIDENCE_ZENITH_ANGLE_B1	DOUBLE	Mean value containing viewing incidence zenith angle average for band B1 and for all detectors
MEAN_INCIDENCE_ZENITH_ANGLE_B2	DOUBLE	Mean value containing viewing incidence zenith angle average for band B2 and for all detectors
MEAN_INCIDENCE_ZENITH_ANGLE_B3	DOUBLE	Mean value containing viewing incidence zenith angle average for band B3 and for all detectors
MEAN_INCIDENCE_ZENITH_ANGLE_B4	DOUBLE	Mean value containing viewing incidence zenith angle average for band B4 and for all detectors
MEAN_INCIDENCE_ZENITH_ANGLE_B5	DOUBLE	Mean value containing viewing incidence zenith angle average for band B5 and for all detectors
MEAN_INCIDENCE_ZENITH_ANGLE_B6	DOUBLE	Mean value containing viewing incidence zenith angle average for band B6 and for all detectors
MEAN_INCIDENCE_ZENITH_ANGLE_B7	DOUBLE	Mean value containing viewing incidence zenith angle average for band B7 and for all detectors
MEAN_INCIDENCE_ZENITH_ANGLE_B8	DOUBLE	Mean value containing viewing incidence zenith angle average for band B8 and for all detectors
MEAN_INCIDENCE_ZENITH_ANGLE_B8A	DOUBLE	Mean value containing viewing incidence zenith angle average for band B8a and for all detectors
MEAN_INCIDENCE_ZENITH_ANGLE_B9	DOUBLE	Mean value containing viewing incidence zenith angle average for band B9 and for all detectors
MEAN_INCIDENCE_ZENITH_ANGLE_B10	DOUBLE	Mean value containing viewing incidence zenith angle average for band B10 and for all detectors
MEAN_INCIDENCE_ZENITH_ANGLE_B11	DOUBLE	Mean value containing viewing incidence zenith angle average for band B11 and for all detectors
MEAN_INCIDENCE_ZENITH_ANGLE_B12	DOUBLE	Mean value containing viewing incidence zenith angle average for band B12 and for all detectors
MEAN_SOLAR_AZIMUTH_ANGLE	DOUBLE	Mean value containing sun azimuth angle average for all bands and detectors
MEAN_SOLAR_ZENITH_ANGLE	DOUBLE	Mean value containing sun zenith angle average for all bands and detectors
MEDIUM_PROBA_CLOUDS_PERCENTAGE	DOUBLE	Percentage of pixels classified as medium probability clouds
MGRS_TILE	STRING	US-Military Grid Reference System (MGRS) tile
NODATA_PIXEL_PERCENTAGE	DOUBLE	Percentage of No Data pixels
NOT_VEGETATED_PERCENTAGE	DOUBLE	Percentage of pixels classified as non-vegetated
PROCESSING_BASELINE	STRING	Configuration baseline used at the time of the product generation in terms of processor software version and major Ground Image Processing Parameters (GIPP) version
PRODUCT_ID	STRING	The full id of the original Sentinel-2 product
RADIATIVE_TRANSFER_ACCURACY	DOUBLE	Accuracy of radiative transfer model
RADIOMETRIC_QUALITY	STRING	Based on the OLQC reports contained in the Datastrips/QI_DATA with RADIOMETRIC_QUALITY checklist name
REFLECTANCE_CONVERSION_CORRECTION	DOUBLE	Earth-Sun distance correction factor
SATURATED_DEFECTIVE_PIXEL_PERCENTAGE	DOUBLE	Percentage of saturated or defective pixels
SENSING_ORBIT_DIRECTION	STRING	Imaging orbit direction
SENSING_ORBIT_NUMBER	DOUBLE	Imaging orbit number
SENSOR_QUALITY	STRING	Synthesis of the OLQC checks performed at granule (Missing_Lines, Corrupted_ISP, and Sensing_Time) and datastrip (Degraded_SAD and Datatation_Model) levels
SOLAR_IRRADIANCE_B1	DOUBLE	Mean solar exoatmospheric irradiance for band B1
SOLAR_IRRADIANCE_B2	DOUBLE	Mean solar exoatmospheric irradiance for band B2
SOLAR_IRRADIANCE_B3	DOUBLE	Mean solar exoatmospheric irradiance for band B3
SOLAR_IRRADIANCE_B4	DOUBLE	Mean solar exoatmospheric irradiance for band B4
SOLAR_IRRADIANCE_B5	DOUBLE	Mean solar exoatmospheric irradiance for band B5
SOLAR_IRRADIANCE_B6	DOUBLE	Mean solar exoatmospheric irradiance for band B6
SOLAR_IRRADIANCE_B7	DOUBLE	Mean solar exoatmospheric irradiance for band B7
SOLAR_IRRADIANCE_B8	DOUBLE	Mean solar exoatmospheric irradiance for band B8
SOLAR_IRRADIANCE_B8A	DOUBLE	Mean solar exoatmospheric irradiance for band B8a
SOLAR_IRRADIANCE_B9	DOUBLE	Mean solar exoatmospheric irradiance for band B9
SOLAR_IRRADIANCE_B10	DOUBLE	Mean solar exoatmospheric irradiance for band B10
SOLAR_IRRADIANCE_B11	DOUBLE	Mean solar exoatmospheric irradiance for band B11
SOLAR_IRRADIANCE_B12	DOUBLE	Mean solar exoatmospheric irradiance for band B12
SNOW_ICE_PERCENTAGE	DOUBLE	Percentage of pixels classified as snow or ice
SPACECRAFT_NAME	STRING	Sentinel-2 spacecraft name: Sentinel-2A, Sentinel-2B
THIN_CIRRUS_PERCENTAGE	DOUBLE	Percentage of pixels classified as thin cirrus clouds
UNCLASSIFIED_PERCENTAGE	DOUBLE	Percentage of unclassified pixels
VEGETATION_PERCENTAGE	DOUBLE	Percentage of pixels classified as vegetation
WATER_PERCENTAGE	DOUBLE	Percentage of pixels classified as water
WATER_VAPOUR_RETRIEVAL_ACCURACY	DOUBLE	Declared accuracy of the Water Vapor model

DATASET DOCUMENTATION: DATASHEETS FOR DATASETS

Here we answer the questions outlined in the datasheets for datasets paper by Gebru et al. [43].

A. Motivation

For what purpose was the dataset created? The dataset was created for unsupervised pre-training in Earth observation. By integrating global coverage, multiple modalities and multiple timestamps, the dataset is intended to serve for diverse applications in remote sensing. The dataset fills the gap between multiple existing pre-training datasets, e.g. domain gap of ImageNet, regional coverage of BigEarthNet [12], single modality of SeCo [4], single timestamp of SEN12MS [13], and patch overlap of both SEN12MS and SeCo.

Who created the dataset (e.g., which team, research group) and on behalf of which entity (e.g., company, institution, organization)? The dataset was created by the lab "Data Science in Earth Observation" at Technical University of Munich and German Aerospace Center.

Who funded the creation of the dataset? The creation of the dataset was funded by the Helmholtz Association through the Framework of Helmholtz AI (grant number: ZT-I-PF-5-01) - Local Unit "Munich Unit @Aeronautics, Space and Transport (MASTR)". The computing resources for benchmark experiments were supported by the Helmholtz Association's Initiative and Networking Fund on the HAICORE@FZJ partition.

B. Composition

What do the instances that comprise the dataset represent (e.g., documents, photos, people, countries)? This dataset only contains satellite images. In addition we provide meta-data for these images, which contain information about data acquisition.

How many instances are there in total (of each type, if appropriate)? The dataset contains 251079 geographical patches, each patch including 3 product types and 4 seasons. In total there are 1M patches each for Sentinel-1 GRD, Sentinel-2 L1C and Sentinel-2 L2A, resulting in 1.5TB as three tar.gz files.

Does the dataset contain all possible instances or is it a sample (not necessarily random) of instances from a larger set? The dataset is a sample of all Sentinel-1/2 satellite images. While the dataset can still be extended, we make it as representative as possible by ensuring global coverage, multiple modalities and multiple timestamps.

What data does each instance consist of? Sentinel-1/2 images along with meta-data captured from the space.

Is there a label or target associated with each instance? No, our dataset is unlabeled. However, each patch is bound with geographical location and acquisition time, thus a match to other labeled maps is possible.

Is any information missing from individual instances? No.

Are relationships between individual instances made explicit (e.g., users' movie ratings, social network links)? Not applicable, though geographic location / acquisition time / product type / other properties can be extracted if needed.

Are there recommended data splits (e.g., training, development/validation, testing)? The dataset is intended for unsupervised pre-training. Users are free to use either the full split or a subset (either a subset of modalities or a subset of geographical patches) based on their targeted applications.

Are there any errors, sources of noise, or redundancies in the dataset? Yes, as mentioned in the data collection section, there are two kinds of noise/redundancies: first, potential overlap around grid cell boundaries; second, potential noise of clouds from inaccurate cloud filtering.

Is the dataset self-contained, or does it link to or otherwise rely on external resources (e.g., websites, tweets, other datasets)? The dataset is self-contained.

Does the dataset contain data that might be considered confidential (e.g., data that is protected by legal privilege or by doctor-patient confidentiality, data that includes the content of individuals' non-public communications)? No.

Does the dataset contain data that, if viewed directly, might be offensive, insulting, threatening, or might otherwise cause anxiety? No.

Does the dataset identify any subpopulations (e.g., by age, gender)? No.

Is it possible to identify individuals (i.e., one or more natural persons), either directly or indirectly (i.e., in combination with other data) from the dataset? No.

Does the dataset contain data that might be considered sensitive in any way (e.g., data that reveals race or ethnic origins, sexual orientations, religious beliefs, political opinions or union memberships, or locations; financial or health data; biometric or genetic data; forms of government identification, such as social security numbers; criminal history)? No.

C. Collection process

How was the data associated with each instance acquired? The data was collected from the publicly available Sentinel-1/2 database.

What mechanisms or procedures were used to collect the data (e.g., hardware apparatus or sensor, manual human curation, software program, software API)? Google Earth Engine with Python were used to collect the data.

If the dataset is a sample from a larger set, what was the sampling strategy (e.g., deterministic, probabilistic with specific sampling probabilities)? The patch locations are Gaussian sampled around a city center (50km) which is uniformly sampled from top-10k populated cities across the globe. The timestamps are sampled from four seasons (dates around Mar 20th, Jun 21st, Sep 22nd and Dec 21st) in the year 2020/2021.

Who was involved in the data collection process (e.g., students, crowdworkers, contractors) and how were they compensated (e.g., how much were crowdworkers paid)? The data was automatically collected and verified by the authors.

Over what timeframe was the data collected? The data was collected by the authors between February and March 2022. The images within the dataset were captured in the year 2020/2021.

Were any ethical review processes conducted (e.g., by an institutional review board)? No.

Did you collect the data from the individuals in question directly, or obtain it via third parties or other sources (e.g., websites)? The data was collected from open sources.

Were the individuals in question notified about the data collection? N/A.

Did the individuals in question consent to the collection and use of their data? N/A.

If consent was obtained, were the consenting individuals provided with a mechanism to revoke their consent in the future or for certain uses? N/A.

Has an analysis of the potential impact of the dataset and its use on data subjects (e.g., a data protection impact analysis) been conducted? N/A.

D. Preprocessing/cleaning/labeling

Was any preprocessing/cleaning/labeling of the data done (e.g., discretization or bucketing, tokenization, part-of-speech tagging, SIFT feature extraction, removal of instances, processing of missing values)? The data was pre-processed online during the collection/downloading process: filtering out cloudy patches and overlapping patches. No further pre-processing was done.

Was the “raw” data saved in addition to the preprocessed/cleaned/labeled data (e.g., to support unanticipated future uses)? No. The cloudy and overlapping patches were removed before downloading.

Is the software used to preprocess/clean/label the instances available? Yes, we use Google Earth Engine with Python which is freely available.

E. Uses

Has the dataset been used for any tasks already? In this paper we use the dataset to benchmark several self-supervised methods on several downstream tasks.

Is there a repository that links to any or all papers or systems that use the dataset? Yes we will organize and maintain all related information at <https://github.com/zhu-xlab/SSL4EO-S12>.

What (other) tasks could the dataset be used for? The main function of this dataset is to provide a pre-training dataset for both the study of self-supervised learning, and specific downstream applications. The dataset can also be used as a baseline for further pre-training datasets in Earth observation. In addition, the dataset can be used directly for applications like image retrieval, domain adaptation and style transfer.

Is there anything about the composition of the dataset or the way it was collected and preprocessed/cleaned/labeled that might impact future uses? We do not unify the orbiting (ascending/descending) of Sentinel-1 data, which should be taken into consideration for SAR related applications. However, the orbiting information can be found in the meta-data and the dataset can be further processed for targeting applications.

Are there tasks for which the dataset should not be used? The authors are not aware of any specific task that should be avoided.

F. Distribution

Will the dataset be distributed to third parties outside of the entity (e.g., company, institution, organization) on behalf of which the dataset was created? Yes, the dataset is publicly available.

How will the dataset will be distributed (e.g., tarball on website, API, GitHub)? The dataset is distributed as tarball on mediaTUM. Access to the dataset can be found at <https://github.com/zhu-xlab/SSL4EO-S12>.

When will the dataset be distributed? Starting from June 2022.

Will the dataset be distributed under a copyright or other intellectual property (IP) license, and/or under applicable terms of use (ToU)? CC-BY.

Have any third parties imposed IP-based or other restrictions on the data associated with the instances? No.

Do any export controls or other regulatory restrictions apply to the dataset or to individual instances? No.

G. Maintenance

Who is supporting/hosting/maintaining the dataset? The dataset is hosted by mediaTUM and supported/maintained by the authors.

How can the owner/curator/manager of the dataset be contacted (e.g., email address)? The authors can be reached at their email addresses: {yi.wang, nassim.aitalibrahham, conrad.albrecht, chenying.liu}@dlr.de, and {zhitong.xiong, xiaoxiang.zhu}@tum.de.

Is there an erratum? If errors are found an erratum will be added.

Will the dataset be updated (e.g., to correct labeling errors, add new instances, delete instances)? Any updates will be posted and the dataset will be versioned.

If the dataset relates to people, are there applicable limits on the retention of the data associated with the instances (e.g., were individuals in question told that their data would be retained for a fixed period of time and then deleted)? N/A.

Will older versions of the dataset continue to be supported/hosted/maintained? Depending on the updates (if there are), we will either continue hosting the older versions or make a clear update log that older versions can be generated from the newest version.

If others want to extend/augment/build on/contribute to the dataset, is there a mechanism for them to do so? Yes, please feel free to reach out to us.

H. Author statement of responsibility

The authors confirm all responsibility in case of violation of rights and confirm the licence associated with the dataset.